Available online at www.sciencedirect.com
SCIENCE DIRECT®
Journal of volcanology and geothermal research
ELSEVIER
Journal of Volcanology and Geothermal Research 3002 (2003) 1–22
www.elsevier.com/locate/jvolgeores

Transient phenomena in vesicular lava flows based on laboratory experiments with analogue materials

N. Bagdassarov [a,*], H. Pinkerton [b]

[a] *Institut für Meteorologie und Geophysik, J.W. Goethe-Universität Frankfurt, Frankfurt am Main, Germany*
[b] *Department of Environmental Science, I.E.N.S., Lancaster University, Lancaster LA1 4YQ, UK*

Received 22 December 2001; accepted 15 July 2003

Abstract

Realistic lava flow models require a comprehensive understanding of the rheological properties of lava under a range of stress conditions. Previous measurements have shown that at typical eruption temperatures lavas are non-Newtonian. This is commonly attributed to the formation and destruction of crystal networks. In the present study, the effects of bubbles on the time-dependent, non-Newtonian properties of vesicular melts are investigated experimentally using analogue materials. The shear-thinning behaviour of bubbly liquids is shown to be dependent on the previous shearing history. This thixotropic behaviour, which was investigated using a rotational vane-viscometer, is caused by delayed bubble deformation and recovery when subjected to changes in shear stress. The viscoelastic transition and the transient flow behaviour of analogue fluids were studied using both a rotational vane-viscometer and oscillatory shear apparatus. These experiments have shown that vesicular suspensions are viscoelastic fluids with a yield strength, power law rheology, and a non-zero shear modulus. These properties are also found in polymer fluids commonly used as analogue materials for lava such as gum rosin. We show that, when materials with this rheology are accelerated in channels, they may be fragmented, and when they flow through a narrowing conduit, pulsating flow can develop as a consequence of a transition from slip to non-slip conditions at the conduit wall. This has important implications both for effusive and explosive volcanic eruptions.

Keywords: lava flow; thixotropy; yield strength; viscoelasticity; gum rosin; foam rheology

1. Introduction

Reliable rheological data are essential for modelling eruptive volcanic processes (Marsh, 1987). However, different rheological models are commonly used in simulations. For example, in some lava flow simulations, lavas are assumed to behave as Newtonian fluids (Keszthelyi and Self, 1998). In others, e.g. Pinkerton and Wilson (1994), Dragoni (1993) and Miyamoto and Sasaki (1998), Bingham behaviour is assumed, and viscoelastic Maxwell behaviour has been used by Dragoni and Tallarico (1996). While there are many circumstances where such approximations can prove useful, there is clearly a need for a reassessment of the appropriateness of different

* Corresponding author. Tel.: +49-69-798-23376; Fax: +49-69-798-23280.
E-mail address: nickbagd@geophysik.uni-frankfurt.de (N. Bagdassarov).

0377-0273/03/$ – see front matter © 2003 Published by Elsevier B.V.
doi:10.1016/S0377-0273(03)00341-X

rheological models in volcanology. In this contribution we present evidence that suggests that there are many circumstances where none of the above rheological models are appropriate. We argue that realistic modelling of many volcanological processes needs to take into account changes in rheological properties during flow caused by reversible structural changes in vesicular or crystalline lavas. The question is how to parameterise their time dependent viscosity and what kind of parameter may be used to quantify the build-up and breakdown of transient structures in magmas.

The temporal variations in lava flow rheology can be caused by one or more of the following: thixotropic effects arising from vesicle deformation (elongation and subsequent change of orientation); viscoelastic properties of the melt matrix itself; and the onset of a dynamic yield strength. We investigated the relative importance of these experimentally. In the first set of experiments we studied the thixotropic properties of bubbly liquids using a rotating shear vane, and in the second set of rotating shear vane experiment we measured the shear-thinning behaviour of a viscoelastic foam. We also used oscillatory torque experiment to investigate the importance of the viscoelastic properties of a bubble-free polymer that is commonly used to simulate lava flows.

As a theoretical introduction to the subject we begin with a brief review of the rheological properties of lavas. This highlights the need for additional experimental measurements on low temperature analogue fluids.

2. Transient rheology of lavas

Rheological properties of lava are a function of the chemistry, temperature, crystallinity and vesicularity of silicate melts of which they are composed. They are also related in a complex way to the degassing and thermal history of a flow (Sparks and Pinkerton, 1978; Marsh, 1981, 1987; Lipman et al., 1985). At temperatures above the liquidus, the viscosity of lava at any given temperature is readily estimated from its chemical composition (e.g. Shaw, 1972). However, most lavas are erupted at temperatures below their liquidus, and suspended crystals and bubbles transform the behaviour of magmas from simple Newtonian fluids to more complex rheological materials (Shaw et al., 1968; Shaw, 1969; Pinkerton and Sparks, 1978; Pinkerton and Norton, 1995; Norton and Pinkerton, 1997). In following discussion, we need to clearly distinguish between the rheology of a melt, by which we mean a fully dense silicate melt or groundmass glass; and lava, which is composed of melt, crystals and bubbles in varying proportions.

Laboratory measurements of the rheological properties of crystalline-rich 1983 Etnean lavas by Pinkerton and Norton (1995) showed that they were Newtonian at temperatures above 1120°C. At lower temperatures, they behaved as pseudoplastic fluids with a yield strength. Laboratory measurements were compatible with apparent viscosities measured on the same lavas in the field. The difference in the rheological behaviour at different temperatures was attributed to their differing crystal and vesicle content. If rheological measurements are conducted at stresses much higher than the yield strength, pseudo visco-plastic rheology is observed. The same lavas subjected to stresses comparable or less than the yield strength exhibit a power low rheology, and at stresses much smaller than the yield strength the 'second' Newtonian viscosity, so-called creep rheology, may be observed (Barnes, 1997). In addition to pseudoplasticity, many melts exhibit time-dependent behaviour. This time-dependent phenomenon arises from shear thinning (thixotropy) or shear thickening (negative thixotropy or rheopectic behaviour) of a viscous fluid subjected to a constant strain-rate (Cheng and Evans, 1965). Traditionally, thixotropy is attributed to structural changes that take place in a material during deformation as a function of time (see review by Barnes, 1997). In this sense, thixotropic behaviour may be understood in terms of microstructural breakdown under increased strain-rates or shear stresses, followed by restoration of structure when these are reduced. In common with previous measurements on Hawaiian lavas (Shaw et al., 1968; Shaw, 1969), Etnean lavas were shown (Pinkerton and Norton, 1995) to be thixo-

tropic at temperatures below 1120°C. During runs at lower temperatures, the viscosity increased on shearing. This rheopectic (shear thickening) behaviour is a consequence of either shear-induced crystallisation (Kouchi et al., 1986) or a dilatancy of crystal grains in shear zones (Smith, 1997).

Pinkerton and Norton (1995) also noted that there was both field and laboratory evidence of viscoelastic behaviour. During the 1983 eruption of Mount Etna, the proximal channel had a central upward bulge of 0.42 m which they argue was caused by a negative second normal stress (i.e. the difference between the axial and the vertical normal stresses; see Spera et al., 1988). Evidence of viscoelasticity was also noted during laboratory measurements on crystalline lavas. There was a distinct lower limit at which it was possible to make realistic rheological measurements. Over a temperature range of less than 6 degrees, the behaviour of the lava changed from a material whose deformation was controlled mostly by viscosity to one in which there was considerable elastic rebound of the spindle during insertion into the lava.

The factors controlling the development of a non-Newtonian rheology in crystallising melts have been reviewed by Pinkerton and Stevenson (1992) and Saar et al. (2001). Pinkerton and Stevenson (1992) concluded that non-vesicular basaltic melts can be approximated as Newtonian fluids at crystal concentrations less than 25 vol%, whereas at higher crystal concentrations, they behave as pseudoplastic materials with a yield strength. One of the reasons for the departure from Newtonian behaviour of crystalline melts is the development of a 3-D framework of crystals. For example, if a lava is composed of crystals with axial ratios of 10:1, a bridging framework can begin to form at concentrations as low as 10–20% (Pinkerton and Stevenson, 1992; Hoover et al., 2001; Saar et al., 2001). This framework, once established, will inhibit flow movement at low stresses, and a yield strength will develop. Once this framework is destroyed by shearing, crystals will become oriented parallel to the main shearing direction and the apparent viscosity will be reduced. One of the interesting consequences of this model is that it can explain not only the reason for the formation of a yield strength and pseudoplasticity in lavas, but also thixotropy. If stresses are reduced, crystals will no longer follow streamlines, and a 3-D framework could be rebuilt.

The effects of bubbles may be even more significant than crystals, and they can induce non-Newtonian behaviour at even lower concentrations. This has been highlighted in recent theoretical and experimental studies of the rheological properties of bubble-bearing magmas (Manga et al., 1998; Stein and Spera, 2002; Rust and Manga, 2002a,b). At low shear stresses, surface tension resists bubble deformation and the bubbles effectively behave as rigid solids. Consequently, the viscosity of bubble-rich fluids is higher than its bubble-free equivalent. However, at high strain-rates, bubbles deform sub-parallel to flow direction and consequently the flow lines are not as highly distorted as they are when the bubbles are spherical. Under those conditions the apparent viscosity is reduced (Stein and Spera, 1992; Pinkerton and Norton, 1995; Manga et al., 1998; Llewellin et al., 2002; Stein and Spera, 2002; Rust and Manga, 2002a,b).

The critical point to emerge from the above discussion is that not only do bubbles and crystals account for a deviation from Newtonian flow behaviour on a shear stress-strain-rate graph, but also both bubble deformation and crystal orientation parallel to flow direction are recoverable. Consequently, lavas containing bubbles will exhibit thixotropic behaviour and lavas with crystals can behave either as thixotropic or rheopectic materials, and possibly both!

The observed elastic behaviour of lavas will either take place at low temperatures when extensive crystal networks are present, or when they contain high bubble contents. Elasticity can develop in vesiculating magmas because, during bubble growth, vesicles become surrounded by a thin melt shell with a significantly reduced amount of volatiles. This volatile-depleted shell will have a relatively high viscosity, as has been observed in decompression experiments using Gum rosin-acetone (Mourtada-Bonnefoi and Mader, 2001) and in rhyolite melts (Stevenson et al., 1997; Stevenson et al., 2001). Another reason for elasticity is a

rim of nucleated crystals around a vesicle. Although the viscosity of magmas with deformable vesicles decreases at high strain-rates $Ca \gg 1$ (Ca is a capillary number, see Appendix) and at large strains (Stein and Spera, 1992; Pinkerton and Norton, 1995; Manga et al., 1998; Llewellin et al., 2002; Manga and Loewenberg, 2001; Stein and Spera, 2002; Rust and Manga, 2002a,b), the highly viscous skin around bubbles may produce an opposite effect. The origin of a thin shell with a high viscosity is due to degassing of the melt. When the temperature T of a melt with volatiles exceeds the glass transition temperature T_g, the bulk of melt will be viscous. However, in the shell around a growing bubble $T < T_g$, because melt will be depleted in volatiles and because T_g decreases with increasing water content (e.g. Stevenson et al., 1997, 2001).

In this paper we consider mostly the effect of bubbles on the time dependent properties of vesicular suspensions. We will show that bubble stretching and deformation processes can explain the observed thixotropic behaviour of lavas.

3. Thixotropy of lava flows and bubble deformation

Thixotropic properties may be important when the shear strain-rate varies in time or across a lava flow section. As a starting point we consider a lava flow as a suspension of bubbles in a melt with thickness h situated on a sloping plane and subjected to a shear stress due to the gravity (Fig. 1). The well known solution of the problem for a velocity $v(z)$ and stress profile σ_{zx} in viscous flow with constant viscosity μ and variable thickness h along the slope length L is:

$$v(z) = \frac{\rho g\left\{\sin\alpha - \frac{dh}{dL}\cdot\cos\alpha\right\}}{2\mu} z(2h-z),$$

$$\sigma_{zx} = \rho g\left\{\sin\alpha\cdot(h-z) - \frac{dh}{dL}\cdot\cos\alpha\right\} - \sigma_Y \qquad (1)$$

where μ is shear viscosity of lava, α is slope angle, ρ is density, h is thickness of a flow, and σ_Y is bulk yield strength (Landau and Lifshitz, 1987; Miyamoto and Sasaki, 1998). The gradient of

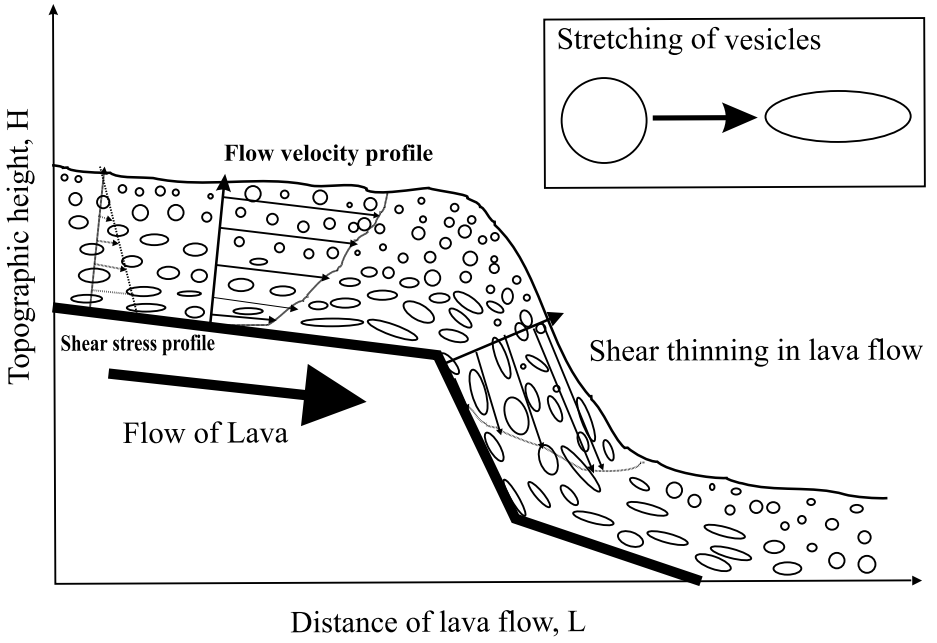

Fig. 1. Sketch of the mechanism of lava flow thixotropy due to bubble stretching and recovery. On shallow slopes the crust of a flow contains spherical to sub-spherical vesicles. If the flow encounters a steep gradient, bubbles are stretched, causing a decrease in apparent viscosity, acceleration of a flow and thinning of the flow.

the underlying ground (sin α) may vary along the distance of a lava flow L which means that a liquid will be subjected to a variable strain-rate. This variation in strain-rate or shear stress profile along the length of lava flow may cause a significant stretching and subsequent relaxation of vesicle shape, and this will affect the apparent viscosity of a flow (Fig. 1). The present study aimed to improve our understanding of about different aspects of transient magma flows. The transient flow of lava may arise from vesicle deformation, or from viscoelasticity of fluid itself, or from non-Newtonian rheology and yield strength due to a high volumetric proportion of vesicles.

As a simple parameter of bubble deformation we introduce an aspect ratio $\lambda = d/D$ of a vesicle, where d and D are the smallest and largest vesicle diameters. This parameter varies from 1 (a sphere) to 0 (a highly elongate ellipse) and may be used as a structural parameter for a lava flow. The dependence of a deformation parameter from a dimensionless shear rate (Capillary number) Ca has been provided elsewhere (Manga et al., 1998; Rust and Manga, 2002b). We can then apply a model of a thixotropic fluid developed by Cheng and Evans (1965), and Cheng (1974, 1986) to a vesicular lava flow. Cheng and Evans (1965) argued that the stress-strain equation depends on the fluid model (for example, see Appendix) and must be completed with a kinetic equation of the structural parameter λ. The general form of this kinetic equation is a rate of shape relaxation $\dot{\lambda}$ as a function of a structural parameter λ, viscosity of a liquid matrix μ and shear strain-rate $\dot{\gamma}$.

$$\frac{d\lambda}{dt} = A\cdot(1-\lambda)^B - C\cdot\lambda\cdot(\dot{\gamma})^E, \qquad (2)$$

where A, B, C, E are constants of a particular fluid (Barnes, 1997). When $B = E = 1$ and $A = \tau^{-1}$ (τ is a characteristic relaxation time of a structure at rest upon a cessation of steady flow, Eq. 2 takes the form of a Frederickson kinetic equation (Bautista et al., 1999). The first term in the right hand side of Eq. 2 is responsible for a recovery of a fluid structure (bubble shape) at rest, the second term defines an equilibrium structure parameter (aspect ratio of a bubble under extension) of a fluid in a flow with a constant shear rate or Capillary number Ca. When $E = 1$ in Eq. 2, the importance of thixotropic effects in a fluid depends on a dimensionless number $(C/A)\cdot\dot{\gamma}$, which is called thixotropic Deborah number (Mujumdar et al., 2002). The combination of the kinetic equation Eq. 2 with a stress-strain relationship of a particular fluid model expressed in terms of strain-stress differential equation (see Eq. A1 in the Appendix) can predict the non-Newtonian behaviour, thixotropic loops and apparent yield strengths in lava flows (Bautista et al., 1999). We define yield-stress as the effective stress above which the viscosity is pseudo-plastic with a break-down structure, and below which the rheology is of a creep-type when an equilibrium structure is still preserved.

In the case of a fluid containing vesicles we may assume that the structural parameter (λ) is a deformation parameter of a vesicle in a sheared fluid, and Eq. 2 may be constructed on the base of laboratory experiments with analogue liquids (Rust and Manga, 2002b). According to their experiments in a steady-state ($\dot{\lambda} = 0$) the deformation parameter depends only on the dimensionless strain-rate or Capillary number $Ca = (a\cdot\mu\cdot\dot{\gamma}/\Gamma)$, where a is an effective diameter of vesicles, μ is a shear viscosity of fluid, and σ is a surface tension of fluid, and the rate of bubble shape restoration after cessation of deformation ($\dot{\gamma} = 0$) exponentially decaying function with the relaxation time of a bubble shape $\tau = (a\cdot\mu/\Gamma)$ (Rust and Manga, 2002b). Thus, Eq. 2 for a fluid containing bubbles may be rewritten as follows:

Table 1
Parameters of thixotropic behaviour of a suspension with ca. 10 vol% of vesicles

	K	m	Reference
Set 1 for Eq. 5	0.625	1.43	Rheological data of Rust and Manga (2002a) for $\varphi \sim 10$ vol%, $\mu_8 = 0.79$, $\mu_0 = 1.12$
Set 2 for Eq. 5	0.784	1.61	Rheological data of Rust and Manga (2002a) for $\varphi > 10$ vol%, $\mu_8 = 0.78$, $\mu_0 = 1.12$
Set 3 for Eq. 3	2.39 ± 0.12	1.20 ± 0.06	Deformation parameter data of Rust and Manga (2002b, fig. 3)
Set 4 for Eq. 3	5.09 ± 0.35	1.32 ± 0.05	Deformation parameter data of Rust and Manga (2002b, fig. 4)

$$\tau\frac{d\lambda}{dt} = (1-\lambda)-\lambda\cdot K\cdot Ca^m, \quad (3)$$

where numerical constant K and exponent m are obtained by fitting the data in fig. 3 from Rust and Manga (2002b), and they are listed in Table 1. In the fitting procedure the differing definition of a deformation parameter (D) from Rust and Manga (2002b) is taken into account. The numerical constant 0.67 in the exponential decay function in Fig. 6 (Rust and Manga, 2002b) is omitted in the present study because of differing definitions of D/a and λ ($a/D \sim \lambda^{2/3}$). Eq. 3 fully describes transient bubble elongation in a shear flow with a dimensionless strain-rate Ca and the rerounding of vesicles when strain-rate is reduced to zero. The same power low dependence of the suspension viscosity as a function of Ca must be observed in a Cross equation (Cheng, 1982). Eq. 3 demonstrates that the deformation parameter λ can be considered as a characteristic of the thixotropic behaviour and the difference in shear viscosity at high ($Ca \gg 1$) and low ($Ca \ll 1$) strain-rates is due to the relaxation of λ. According to the definition of thixotropy given by Cheng (1982), the thixotropic material can transform between different structural states under applied shear rate or strain. The rate of recovery in thixotropic material depends on the current structural level which is the case of Eq. 3. According to the definition of the thixotropic Deborah number, if $K\cdot Ca^m \gg 1$, thixotropic effects should be considered in predicting the stress response (Mujumdar et al., 2002). Although the relaxation time of bubble rerounding depends only on fluid properties, the rate of this process depends on the achieved deformation parameter λ, and Ca. In equilibrium the deformation parameter λ_e is solely a function of Ca:

$$\lambda_e = (1 + K\cdot Ca^m)^{-1}. \quad (4)$$

The shear viscosity of lava with vesicles which appeared in Eq. 1 is a viscosity of a bubbly suspension $\mu = \mu_{silicate\ melt} * \mu_{rel}$. Material parameters in the strain-stress differential equation such as viscosity μ have to be dependent not only on a volume fraction of crystals or bubbles (see Llewellin et al., 2002) but also on a shape (structure) parameter λ. Indirectly this information has been obtained in experiments of Rust and Manga (2002a). The relative viscosity of a dilute suspension has been obtained from the experiments with analogue liquids:

$$\mu_{rel} = \mu_\infty + \frac{\mu_0-\mu_\infty}{1 + K\cdot Ca^m}, \quad (5)$$

where μ_∞ and μ_0 are suspension relative shear viscosities at $Ca \gg 1$ and $\ll 1$, respectively (Rust and Manga, 2002a). The estimated values of μ_∞ and μ_0 for a suspension with ca. 10 vol% of vesicles are listed in Table 1. The difference in the exponents and coefficients in Eqs. 2 and 3 taken from Rust and Manga (2002a,b) may be attributed to the fitting procedure and experimental errors of the Ca estimations. In theory, they should coincide (Cheng, 1982). For convenience we used K and m from fitting of viscosities data (Rust and Manga, 2002a,b). In a steady-state under constant Ca, the deformation parameter λ is a unique function of Ca which follows from the right hand side of Eq. 3. The time-dependence of μ_{rel} is therefore due to the time dependence of λ, which obeys Eq. 3. Thus, the temporal variation of lava flow on a slope of a volcano with a known topography including the thixotropic effect of the vesicles elongation and rerounding (non-Newtonian rheology of a flow) may be estimated by solving Eqs. 1, 3 and 5.

In Section 4 we present the results of a series of rheological measurements on laboratory analogue materials. Measurements have been made using torsion deformation and a rotational vane-viscometer (Table 2). In these experiments we deter-

Table 2
Materials used in laboratory experiments with rotational viscometer and torsion oscillatory shear

Sample	Temperature	Measured properties	Fluid properties
Aqueous foam	25°	Yield strength: step in strain-rate, step-in-shear strain	Air bubbles ca. 90 vol%
Golden syrup	25°C	Stress relaxation: step in strain-rate, rotational viscometry	Air bubbles ca. 10 vol%
Gum rosin	25–60°C	Oscillatory shear: shear modulus, internal friction	Homogeneous liquid

mined yield strengths, frequency dependent shear moduli and viscosities and used these to construct a viscoelastic model of a bubble-bearing liquid that can be applied to lava and magma flow modelling.

4. Experiments

4.1. Thixotropy of bubbly liquid

For many fluids, the apparent viscosity varies with time as well as with applied shearing stress. There are two possible explanations for this behaviour. One relates to bubble deformation; the other to crystal interaction. During the initial flow of multiphase viscous fluids, elongate particles may form a bridging framework tending to align along the flow lines. This will decrease the bulk viscosity, resulting in thixotropic (shear thinning) behaviour as we demonstrated in Section 3. For thixotropic materials, the apparent viscosity returns to the unsheared value when the sample is left undisturbed for a sufficient time for the structure to become re-established. When modelling processes that operate in a step-wise manner, for example during periodic eruptions or surges in lava flows, or when lavas move from shallow to steep slopes, the yield strengths and apparent viscosities can change.

Controlled strain-rate experiments on bubbly non-surfactant fluids using a rotational viscometer were used to investigate the thixotropic behaviour of vesicular melts. In these experiments a suspension of golden syrup with ca. 10 vol% by volume of air bubbles were used.

On a stress-strain-rate plot the strategy of experiments may be explained by referring to Fig. 2. The general dependence of shear stress on strain-rate of melt containing ca. 10 vol% of vesicle can be obtained from Eq. 5:

$$\sigma = \frac{\Gamma}{a}\cdot\left(\mu_\infty + \frac{\mu_0-\mu_\infty}{1+K\cdot Ca^m}\right)\cdot Ca, \qquad (6)$$

where surface tension at the bubble-fluid interface $\Gamma\sim 0.08$ N/m and $a\sim 4$ mm. Eq. 6 is valid for

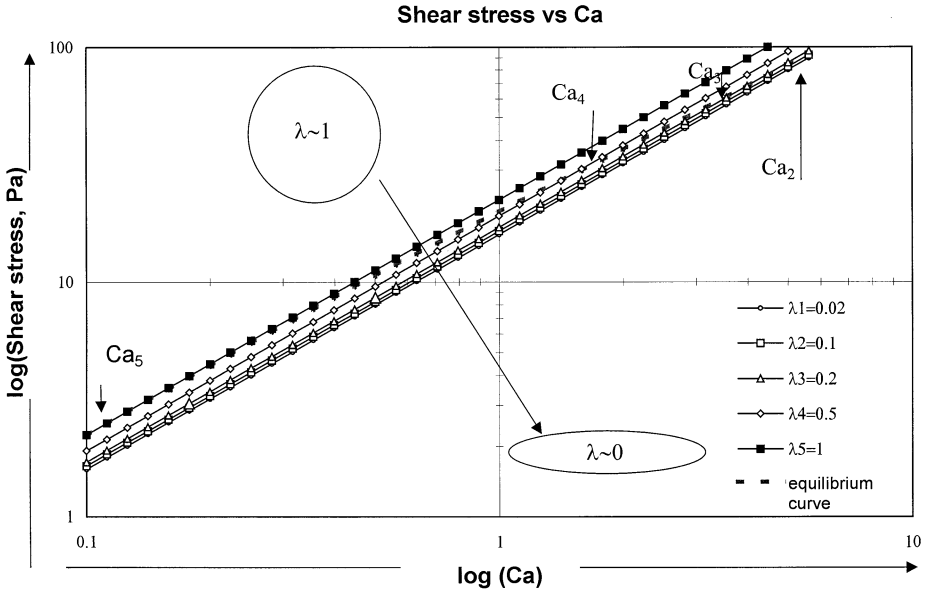

Fig. 2. Principle of isostructural ($\lambda = const$) and equilibrium viscosity measurements using a starting suspension with differing bubble stretching parameter λ. The family of stress–strain-rate curves characterises the viscosity of a fluid with constant bubble elongation parameter λ (Eq. 6). Along each curve λ is constant. By contrast, the equilibrium stress–strain-rate curve represents the data corresponding to a differing $\lambda(Ca)$ according to Eq. 6 (marked by arrows). Parameters K and m are taken from Table 1, set 1. $\mu_\infty = 0.78$, $\mu_0 = 1.12$ are calculated from Rust and Manga (2002a) for $\varphi\sim 10$ vol%.

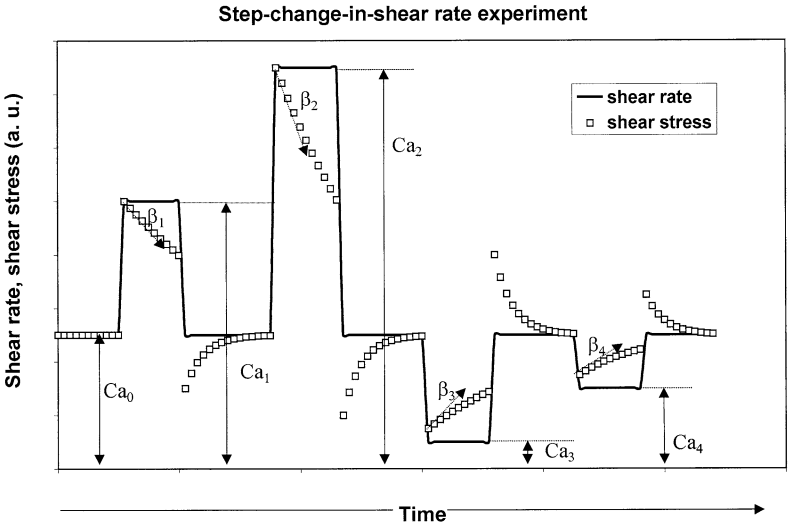

Fig. 3. Principle of step-change in strain-rate experiment using a rotational vane-viscometer (redrawn from Cheng, 1986). The equilibrium λ corresponds to Ca_0. The λ changes after imposing positive (Ca_1, Ca_2) and negative (Ca_3, Ca_4) steps in strain-rate. The rate of stress relaxation β is proportional to the step amplitude in Ca and relaxation of rate of $\dot{\lambda}$.

long run experiments, when the deformation parameter attains a steady-state value λ_e (see Eq. 4). The nature of the viscosity dependence of shear viscosity on Ca lies in the variation of λ. In non-steady-state the viscosity of a suspension depends on a non-steady-state $\lambda;(t)$: $\mu \sim \mu_\infty + (\mu_0 - \mu_\infty)\cdot\lambda$. Thus, the family of curves may be plotted as follows:

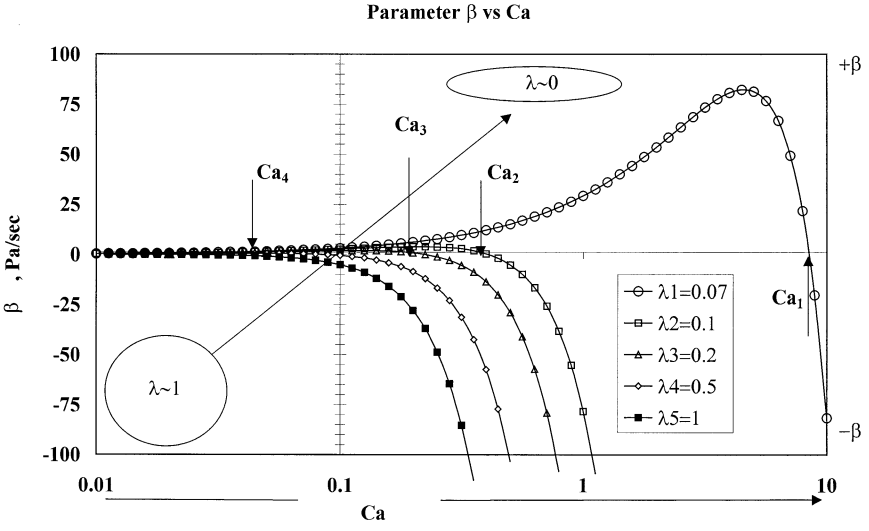

Fig. 4. The rate of change of stress at constant strain-rate as a function of structural parameter λ. For suspensions of bubbles λ characterises a stretching state of a vesicle. Curves represent the relationship $\beta = (d\sigma/dt) = (\Gamma/a)\cdot(\mu_0 - \mu_\infty)\cdot\dot{\lambda}\cdot Ca$, where $\dot{\lambda}$ calculated using Eq. 3. Parameters K and m for calculation of $\dot{\lambda}$ are taken from Table 1, set 1. $\mu_\infty = 0.78$, $\mu_0 = 1.12$ are calculated from Rust and Manga (2002a) for $\varphi \sim 0.1$. Arrows indicate Ca, at which $\beta(Ca) = 0$.

$$\sigma = \frac{\Gamma}{a}\cdot[\mu_\infty + (\mu_0 - \mu_\infty)\cdot\lambda]\cdot Ca \qquad (6A)$$

This family of stress-strain-rate relationships characterises the rheology of a bubbly liquid. Each curve in this family corresponds to a certain stretched bubble shape λ (Fig. 2). The equilibrium or measurable curve intersects the isostructural curves.

If the measurement lasts long enough and a steady-state value of λ is attained, then the measured viscosities are on the equilibrium curve (Fig. 2). But immediately after a step-change in strain-rate, the point moves on a curve with a constant λ. After a certain time the stretching parameter λ drifts to another steady-state value (according to Eq. 2) and the point moves on the stress-strain-rate map from the curve with one value of λ to another.

Finally, the equilibrium viscosity curve representing data for differing structural parameters of a thixotropic liquid or for differing values of the stretching parameter of bubbles may be constructed on the base of step-change in strain-rate experiments. The method of testing for thixotropic behaviour is described by Cheng (1986) and illustrated in Fig. 3. After a step-change in strain-rate the suspension tends to attain another value of the deformation parameter and the shear stress decays with time. The step-change in strain-rate was repeated for a range of reference strain-rates and a range of steps in strain-rates. The thixotropic properties of the bubble bearing fluid can be characterised by a map of parameter $\beta = (d\sigma/dt)_{\dot\gamma}$, the rate of change of shear stress at constant strain-rate. A general view of the β-strain-rate relationship for a suspension with ca. 10 vol% based on experimental data of Rust and Manga (2002a,b) vesicles is presented in Fig. 4. Positive and negative β correspond to positive and negative steps in step-change in strain-rate. The intersection of the β curve with the x-axis is a reference strain-rate when $\beta \equiv 0$.

During the first set of experiments, a Haake RV3 rotational vane-viscometer was used to determine whether aerated Golden Syrup behaves as predicted by the thixotropic model of Cheng and Evans (1965). The Golden Syrup, which contained ca. 10 vol% of air bubbles, has a Newto-

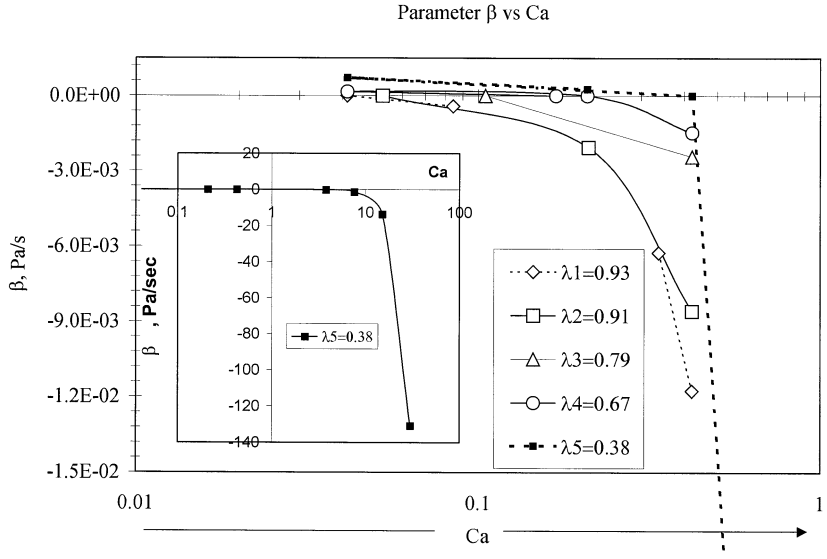

Fig. 5. Shear stress relaxation rate from starting strain-rate (numbers in legend column) to a final strain-rate. Results of measurements of parameter β in suspension of Golden syrup with ca. 10 vol% of air bubbles using a step-strain-rate method. Numbers in the legend are initial strain-rates corresponding to $\beta = 0$. The figure is similar to the theoretical prediction of parameter β for thixotropic fluids shown in Fig. 4. The insert shows data at $Ca \gg 1$. The deformation parameter λ is calculated using Eq. 3 and parameters K and m from Table 1, set 4.

nian viscosity of 10^2 Pa s at 20°C. Bubbles were introduced, using a controllable compressed air injection system, through sintered glass that formed the base of the vessel containing the fluid. The volume fraction of vesicles has been estimated from a volume increase after aeration. The average size of vesicles was ca. 2–4 mm. The aerated Golden Syrup was deformed under a constant strain-rate (constant rotational speed of the vane was converted to the strain-rate). The estimated strain-rates varied from 0.26 to 2.65 s^{-1} for a sufficient length of time to ensure a constant apparent viscosity and a bubble deformation parameter λ. The measured torque was monitored as a function of time after each step in applied strain-rate and converted to a shear stress using a calibrated rotational vane-viscometer. The structural parameter (or bubble elongation in these experiments) attained a steady-state value at this point. A step-change in strain-rate was applied and a time-dependent shear stress was then monitored. The time derivative of the shear stress (β Pa/s) immediately after a step-change in strain-rate is a function of the step amplitude in strain-rate. The step-change in strain-rate can be performed at either increasing or decreasing step-changes of different amplitude. The increasing and decreasing steps in strain-rate were performed in a vane-viscometer from 0.26 to 2.65 s^{-1}. Rotation rates were converted into strain-rates using a viscometer head calibrated using a set of standard fluids with viscosities in the range 1–60 Pa s (Corning Corp.®).

Fig. 5 shows the results for Golden Syrup at 20°C containing about ca. 10 vol% bubbles, and it clearly demonstrates the effect of a decrease in shear stress rate β (Pa/s) as a function of strain-rate. The number in the legend indicates a starting (reference) strain-rate at which the shape of bubbles was steady-state.

The similarity of the family of curves in Figs. 4 and 5 indirectly confirms the idea of the thixotropic nature of bubble suspensions. In recent work by Llewellin et al. (2002) the effect of a dynamic capillary number Cd on the transient rheology of vesucular suspension has been studied. The authors performed experiments with linear increase and decrease of Ca. In this case $\beta = (d\sigma/dt) = (\Gamma/a)\cdot(\mu_0 - \mu_\infty)\cdot\dot{\lambda}\cdot Ca + (\Gamma/a)\cdot(\mu_0 - \mu_\infty)\cdot\lambda\cdot Ca\cdot\tau\cdot Cd$. In our approach the second term of this relationship is set to 0, because the experiments were performed with a constant shear rate or Ca.

From field observations of Etna basaltic lava flows, the width and thickness of lava flow change with topographic relief. This may be accompanied by changes in lava rheology, which is sensitive to both bubble and crystal content. On shallow slopes, when a lava flow moves relatively slowly, the shape of bubbles achieves an equilibrium spherical form. On steeper slopes, when a flow accelerates, bubbles become stretched due to increased shear stresses within the characteristic time scale $\tau = (a\cdot\mu/\Gamma)$, where μ is the Newtonian shear viscosity of the bulk melt, a is the radius of a gas bubble and Γ is the surface tension at the interface between the gas and melt. At the point when a lava flow accelerates, the main stretching of vesicles occurs. Thus the dependence of the slope angle as a function of time may be important to predict the decrease in apparent viscosity of a lava flow. The change in speed accompanying a change in gradient causes changes in bubble shape that can be calculated from the Capillary number Ca (Pinkerton and Norton, 1995; Manga et al., 1998), and the effect of this on rheology has been studied by Llewellin et al. (2002) who recognised the effect of flow variations on rheology via dynamic Capillary number Cd (see Appendix). In an accelerating lava flow, the shear viscosity and shear stresses may decrease at a rate β because of bubble stretching. In thixotropy terms, this means that the liquid changes to a new value of the structural parameter or the elongation shape of bubbles λ according to a new value of the strain-rate $\dot{\gamma}$ or Ca (see Eq. 3). Decrease of the apparent viscosity under shear as a function of time is a consequence of the coupling between fluid structure, in our case bubble shape λ, and viscosity. Numerically this situation has been modelled by Manga and Loewenberg (2001). Thus, in lavas and magmas containing gas bubbles the thixotropic effect may stem from the fact that gas bubbles tend to be stretched during accelerated shear flow.

Comparing Figs. 4 and 5 we conclude that the

coupling between shear stress and viscosity may be due to changes in the internal 'structural parameter' of the flow or deformation of gas bubbles. The shear stress relaxation rate associated with bubble stretching and subsequent relaxation depends on a final strain-rate. The laboratory result on Golden Syrup demonstrated the effect of bubble stretching on a shear stress caused by the abrupt change in a shear strain-rate which may be important for a lava that flows over changing topography.

4.2. Viscoelastic model of foam

Magmas and lavas during vigorous degassing are highly porous materials. As noted previously, the presence of vesicles and crystals in a melt suspension results in both a yield strength (Hoover et al., 2001) and viscoelasticity (James et al., 2004). In the present section we describe how a rotating vane-viscometer can be used to measure yield strengths and viscoelastic properties (shear modulus and shear stress relaxation time) in an analogue foam.

The viscoelastic response and yield strength of fluids was measured using a Haake Rotovisco RV3 rotational vane-viscometer by using the 'imperfection' of a torque spring viscometer (Cheng, 1986). If a fluid is elastic below a certain level of shear stress, then, after applying a step-change in strain-rate, the spring torque will increase linearly with time. From the slope of a shear stress–time line the stiffness of a viscometer spring s may be estimated, e.g. the angle of spring deformation $\dot{\gamma} \cdot t = T/s$, where T is a measured torque (Nm) and s is a vane spring stiffness constant (Nm/rad). Shear stress calculated from $\sigma = T/K$, where K is a geometric factor of the vane in m^3 (Liddell and Boger, 1996). The geometric parameters of the vane used in experiments are as follows: blade length = 0.06 m, blade diameter = 0.04 m, calculated K including corrections to the shaft diameter

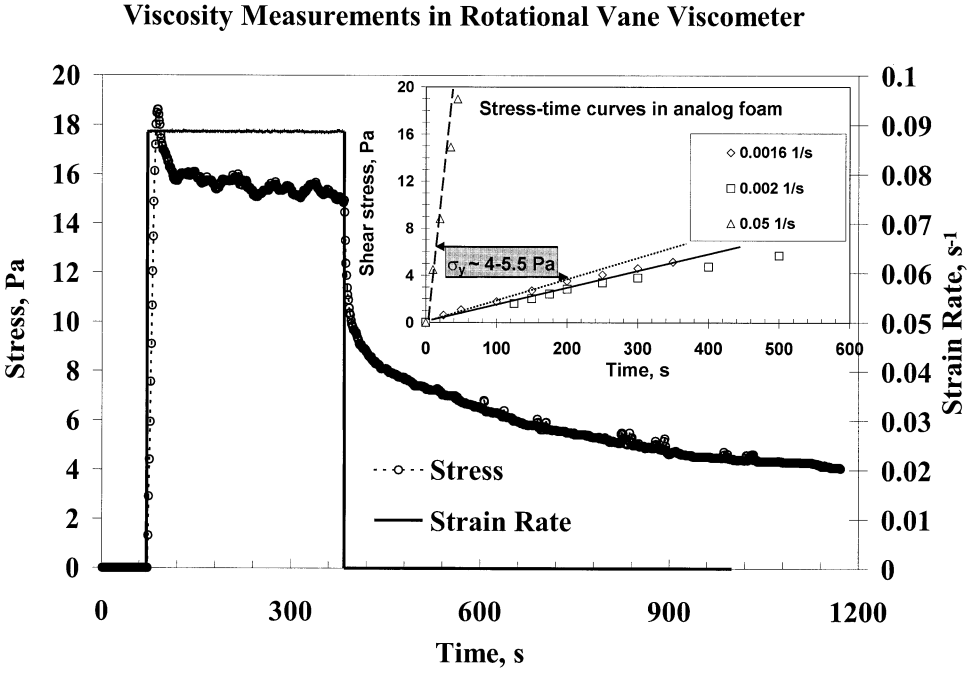

Fig. 6. Viscoelastic response of a foam material with 90 vol% of vesicles to a step function of a strain-rate $\dot{\gamma}$. The insert shows the start of experiments at different strain-rates. The stress corresponding to the deviation from a linear deformation corresponds to a yield strength. The shear modulus may be estimated from a linear response slope. The decay of shear stress after cessation of strain-rate provides a Maxwell relaxation time of viscoelastic behaviour.

(0.004 m) and the excess immersed depth beyond the blades (0.0065 m) is 1.845 10^{-3} m^3 (Avramis and Turian, 1991). During elastic deformation the vane is stationary relative to the sample fluid, the shear stress is $\sigma(t) = \dot{\gamma} \cdot t \cdot s/K$. From this linear deformation a stiffness constant may be estimated (s/K = ca. 8.6 Pa) in our case. The stress value where torque starts to deviate from a straight line corresponds to the static yield strength of a fluid (see insert in Figs. 6 and 7). It corresponds to a transition from elastic to viscoelastic response because of the existence of a yield strength. At high starting shear rates it is unobservable because of a limiting stress–time resolution. When the yield strength is reached elastic stress ceases, and there is relative motion between the vane and the testing fluid at a rate equal to the imposed strain-rate (Liddell and Boger, 1996). The maximum overshoot defines a dynamic yield strength (Liddell and Boger, 1996). Once it has attained a maximum value, the shear stress relaxes exponentially reaching the value of a viscous stress $\sigma = \mu \cdot \dot{\gamma}$, where μ is a Newtonian shear viscosity. This corresponds to the transition between viscoelastic to fully viscous behaviour (Fig. 7). The stress evolution during viscoelastic flow is dependent on material properties (relaxed shear viscosity μ and unrelaxed shear modulus G) as well as on the applied shear rate. The unrelaxed shear modulus can then be calculated from μ and τ, where μ and τ are measured from the stress evolution curve and relaxed shear stress. When strain-rate is reduced to zero, the stress falls exponentially with a time constant $\tau = \mu/(G + s/K)$ (Fig. 7).

The viscoelastic properties of shaving foams containing about 90 vol% of bubbles (size $a \sim 1$ mm) were measured using the above technique at strain-rates from 0.08 to 0.16 s^{-1} with a Haake Rotovisco RV3 rotational viscometer. The porosity of foam has been estimated from the volume–weight measurements. The foam under testing contained surfactants and the rheological properties may change with time due to devolatilisation (Bekkur and Scrivener, 1998). From the observations of a foam in the viscometer, a noticeable change in vesicle size and ageing of shaving foams occurs only after 3–4 h. Our experiments lasted less then 1 h.

A typical stress-strain time curve obtained using

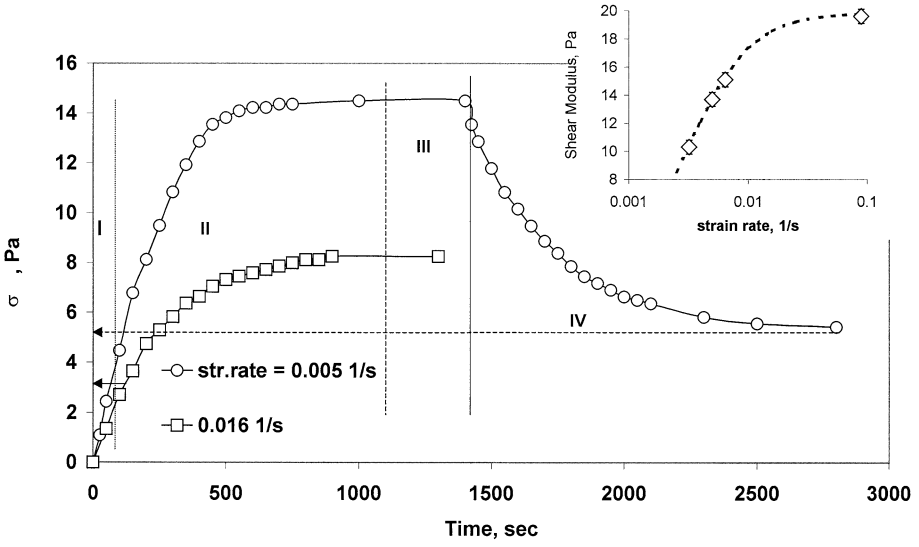

Fig. 7. Response of a foam to a pulse of a strain-rate: (I) elastic regime of foam deformation; (II) viscoelastic response above a yield strength level; (III) viscous flow with a constant viscosity; (IV) exponential decay of shear stress. The insert show a strain-rate dependent shear modulus as a result of shear thinning behaviour the estimated shear modulus from Maxwell relationship $\tau = \mu/G$. The decaying of shear stress after cessation of a strain-rate depends on the previous strain-rate and the stiffness constant of the vane-viscometer. The fitting line in the insert is $G(Pa) = 19.84 \cdot ((\tau\dot{\gamma})^m/1 + (\tau\dot{\gamma}))^m$, $m = 1.6$ and $\tau = 333$ s.

a rotational vane-viscometer is shown in Fig. 6. The plot represents a stress response of shaving foam for a step in strain-rate. The shear modulus G_∞ in the shaving foam is $\sim$20 Pa (insert of Fig. 7), and was estimated from a stress relaxation curve ($\tau\sim$8.7 s) and measured shear viscosity μ (172 Pa s). A yield strength has been measured from a deviation of the stress–strain time curve from a linear dependence at the start of rotation (see Fig. 6) to be 3.5–4 Pa. The yield strength determined as a residual stress remaining after cessation of the applied strain-rate is 4 Pa.

Yield strength is a stress below which the material may be deformed only elastically $\sigma = G\cdot\gamma$ and above which material starts to flow $\sigma = \sigma_Y + \mu\cdot\dot{\gamma}$. Shear modulus G measured at high strain-rates in dynamic shear experiments is G_∞. The insert in Fig. 7 shows the dependence of shear modulus on the strain-rate. After cessation of strain-rate the shear stresses decay not to 0 but to a finite value of static yield strength $\sigma_Y\sim$4–5 Pa (Figs. 6 and 7). The relaxation time of shear stresses to 'residual' shear stress is determined by the shear modulus of the foam and static deformation of the viscometer spring T/S, and viscosity of a foam. The static yield strength estimated from shear stress increase and decrease is about the same, but the time constant of stress decay depends on the previous strain-rate (Ca and λ of vesicles in foam), i.e. on the actual viscosity of the fluid which turns to be strain-rate dependent. By comparison, a yield strength measured in protein foams with ca. 20 vol% porosity is about 40 Pa (Pernell et al., 2000). In laterite suspension with 35 vol% porosity the measured yield strength is 0.65 Pa (Turian et al., 1997). For oil–water foams with a porosity from 75 to 98% the yield strength varies from 4.9 to 101 Pa, respectively (Princen and Kiss, 1986). In lava rheology the nature of yield strength has been postulated and studied as an effect of growing crystal concentration. (Hoover et al., 2001). The effects of vesicle concentration and gas overpressure on the yield strength and non-zero shear modulus has not yet been fully appreciated by volcanologists. The nature of a yield strength and non-zero shear static modulus in foams is different, but may have a relation to the case of a decompressed magma with high volume fraction of vesicles. Non-zero shear moduli in high porosity foams arise because their shear modulus is proportional to the overpressure in pores $G\sim\Delta P$ and is about 3 times larger than the corresponding yield strength (Princen and Kiss, 1986).

In Fig. 8 we present results of shear viscosity measurements of an aqueous shaving foam as a function of strain-rate. The non-Newtonian dependence of viscosity is a consequence of the

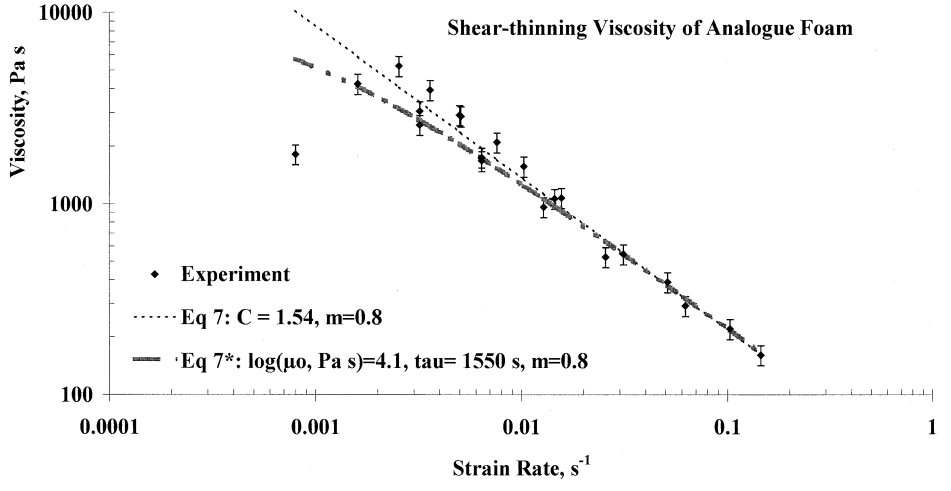

Fig. 8. strain-rate dependence of shear viscosity of a foamed material: $\mu\propto(\dot{\gamma})^{-0.8}$ obtained from rotational viscometry on a shaving foam with ca. 90 vol% of bubbles.

shear-thinning behaviour of the foam. The data in Fig. 8 may be fitted either to a linear regression in a double logarithmic plot:

$$\log(\mu,\ \text{Pa s}) = C - m \cdot \log(\dot{\gamma}), \tag{7}$$

or to a Cross model

$$\mu = \frac{\mu_o}{1 + (\tau \cdot \dot{\gamma})^m}, \tag{7A}$$

where μ_o and m are empirical constants. Eq. 7A is similar to the term for the viscosity in the r.h.s. of Eq. 6A. Instead of a strain-rate independent Newtonian behaviour, our experiments indicate a power law viscosity dependence on strain-rate with the exponent $m \sim 0.8$ (Fig. 8). It means that applying larger strain-rates to the foamed material the resulting shear stress remains practically constant $\sigma \sim (\dot{\gamma}^{0.2}$.

4.3. Oscillatory shear in Gum Rosin

This section deals with the viscoelasticity of a homogeneous liquid and demonstrates the importance of strain-rate dependence of shear modulus in the glass transition temperature range. It is highly desirable that the viscoelastic transition of analogue liquids used in laboratory experiments for modelling magma and lava flows mimics the viscoelastic transition of lava, otherwise the transient flows studied in the laboratory do not represent similar flows of lava and magma. Laboratory modelling of flow fragmentation (Phillips et al., 1995) demonstrated a number of transitional flow phenomena of foams. One of these is periodic stick and slip boundary conditions on the wall of a shock tube and detached flow in the tube centre. This could be a result of combined viscoelastic and plastic properties of the foam used in their experiments. This can be studied using dynamic oscillatory shear to investigate the yield strength and transient response of analogue materials.

Gum rosin, an anelastic organic polymer at room temperature, has been used in shock tube experiments (e.g. Phillips et al., 1995). The viscosity of Gum rosin with dissolved acetone in the temperature range 20–40°C mimics the viscosity of rhyolite melt with dissolved water. Under decompression from acetone saturated pressure to vacuum the dissolved acetone exsolves and a foam forms. The annular flow of the foam in a shock tube is similar to the flow of decompressed magma in a volcanic channel. To what extent do the viscoelastic properties of Gum rosin influence the character of a flow in a shock tube?

In order to answer this question a series of torsion oscillatory shear experiments have been carried out on Gum rosin samples. A detailed description of the apparatus may be found elsewhere (Bagdassarov, 2000; James et al., 2004). In our experiments, gum rosin was melted at ca. 100°C, inserted in an 8-mm-diameter paper tube and cooled to room temperature. The cylinders of Gum rosin were then fixed between two Al_2O_3 rods in the torsion apparatus and measurements of shear modulus and internal friction were made in the temperature range 20–60°C and in the frequency range 20–0.001 Hz.

In Fig. 9A,B the results of the frequency (or strain-rate) dependent complex shear modulus and internal friction of Gum rosin are presented. The unrelaxed shear modulus of Gum rosin is ca. 2.3 ± 0.1 GPa. From these data the maximum of anelastic behaviour of this polymeric material is 50°C at 2 Hz and 40°C at 1 Hz which corresponds to a maximum of the imaginary component of shear modulus plotted as function of frequency (Fig. 9B). Even at the highest temperature (60°C) and lowest frequencies (0.002 Hz) used in the experiments, the shear modulus does not tend to 0. The plateau can be explained by the existence of a yield strength, because the low frequency non-zero shear modulus in fluids and suspensions is often correlated with a yield strength (Nguyen and Boger, 1992; Liddell and Boger, 1996). See Fig. 9A for $G \sim 0.1 \div 0.2$ GPa for Gum rosin at temperatures $> 50°$ well above the viscoelastic transition.

4.3.1. Application to shock tube experiments

In the shock tube experiments performed by Phillips et al. (1995), explosive eruptions are simulated by decompressing a system containing Gum rosin dissolved in acetone. During explosive events in the shock tube, fragments of foam of length L detached from the inner surface of a

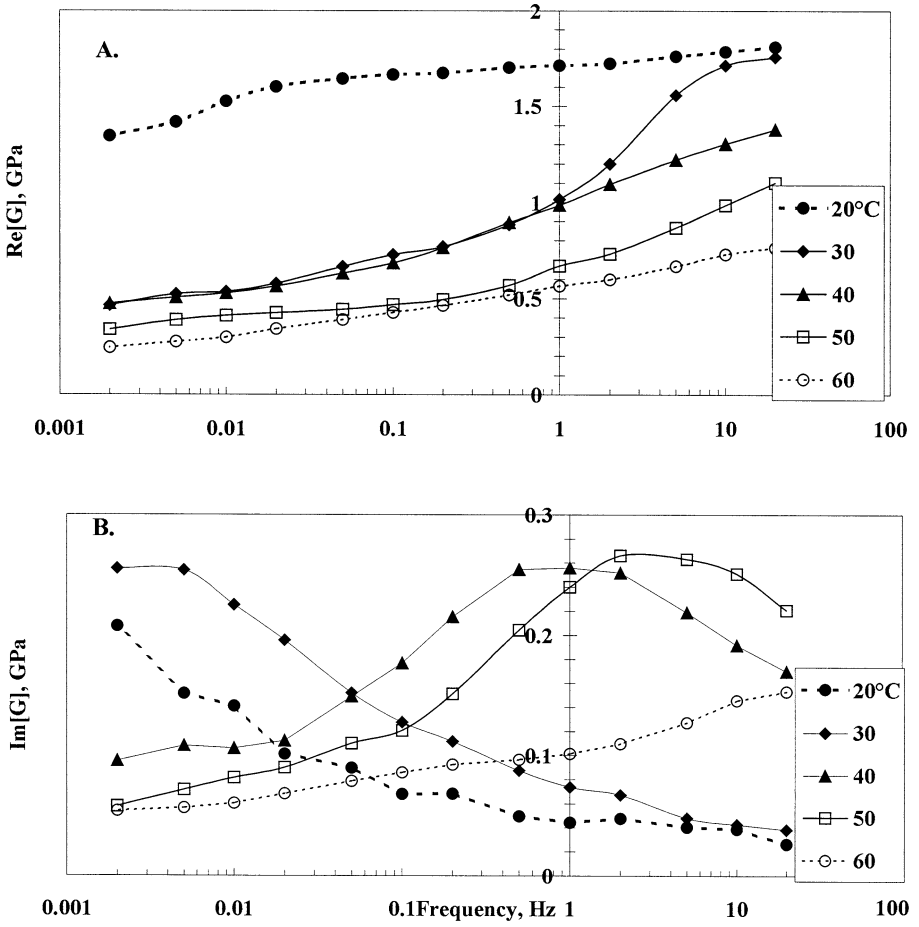

Fig. 9. (A). Real, and (B) imaginary components of shear modulus in Gum rosin sample measured using a torsion deformation device. The strain of oscillatory shear is $\sim 10^{-5}$. Maximum of imaginary component corresponds to the frequency of viscoelastic transition. Non-zero real component of shear modulus at low frequencies may interpreted as a yield strength (Nguyen and Boger, 1992; Liddell and Boger, 1996).

tube (of radius R) and accelerated upwards. If a foam with a liquid density ρ and liquid fraction φ possesses a yield strength (σ_y), the forces acting against the upward force are the weight of a foam fragment ($\rho \cdot L \cdot \pi R^2 \cdot g \cdot \varphi$) and the force of the wall attachment due to a yield-stress ($\sigma_Y \cdot 2\pi R \cdot L \cdot \varphi$). When a fragment detached from the wall, the force acting on a fragment due to the decompression is larger than the sum of two forces slowing down a fragment: $\Delta P \cdot \pi R^2 > \rho \cdot L \cdot \pi R^2 \cdot g + \sigma_Y \cdot 2\pi R \cdot L$, where ΔP is a driving pressure difference in a conduit with a cross section radius R. Consequently, the maximum length of a typical fragment is $L_{max} \approx (\Delta P/(\rho g + (2\sigma_Y)/R) \cdot \varphi)$. At $\Delta P = 10^5$ Pa, $\sigma_Y = 1\text{–}2 \cdot 10^7$ Pa, $\varphi = 5 \cdot 10^{-3}$, $R = 0.01$ m, then $L_{max} \sim 0.5\text{–}1$ cm. Here, the value of σ_Y is taken as a second plateau value of the shear modulus (Fig. 9A) at low frequencies for Gum rosin without dissolved acetone and divided by a factor 10–20 (Nguyen and Boger, 1992). This shear modulus value may be significantly higher than G for Gum rosin acetone foams.

5. Discussion and conclusions

(1) Our experiments using analogue fluids have shown that bubbly suspensions are thixotropic,

viscoelastic fluids with yield strengths. Previous measurements have revealed that vesicular lavas and magmas have similar properties. The effective parameter that may describe the temporal changes in structure is the deformation parameter of vesicles during flow λ. In a lava flow that moves from a shallow to a steep slope, thixotropy causes a decrease in apparent viscosity. The response of a lava to a pulse of an applied strain-rate may be modelled as follows. For a slope ca. 20–25°, lava density 2.5–2.3 10^3 kg/m^3, lava flow thickness 1 m, and melt viscosity 10^6 Pa s, a typical strain-rate according to Eq. A2 will be $\sim 10^{-2}$ s^{-1}. If $\Gamma \sim 0.3$ N/m $a \sim 3\ 10^{-2}$ m, the typical $Ca \sim 10^3$. The dependence of shear viscosity on Ca is given by Eq. 5, K and m parameters for $\phi \sim 10$ vol% are cited in Table 1, set 1. The viscosity of the suspension develops with time from an initial value to a final value according to Rust and Manga (2002a). At $t = 0$ when a strain-rate was applied, viscosity corresponds to $Ca = 0$ (vesicles were not deformed), and at the end it corresponds to $Ca = (a \cdot \dot{\mu} \cdot \gamma / \Gamma)$, where μ is the viscosity of a fully dense fluid phase. The relaxation of λ is given in Eq. 3, K and m parameters are from Table 1, set 4. For viscoelastic stress relaxation, the Maxwell body model has been used: $\dot{\sigma} = G \cdot (\dot{\gamma} - (\sigma/\mu))$. For thixotropic shear stress relaxation we used $\beta = \dot{\sigma} = (\Gamma/a) \cdot (\mu_0 - \mu_\infty) \cdot \dot{\lambda} \cdot Ca + (\Gamma/a) \cdot (\mu_0 - \mu_\infty) \cdot \lambda \cdot Ca \cdot \tau \cdot Cd$. Initial conditions for viscoelastic response $\sigma(t = 0) = 0$, for thixotropic response $\sigma(t = 0) = \mu \cdot \dot{\gamma}$. These equations have been solved numerically using an evolution method. In Fig. 10 we present stress-time curves of viscoelastic, thixotropic and combined responses for a pulse of strain-rate. Relaxation of the deformation parameter λ from 1 to 0 corresponds to a change in the viscosity and shear stresses in a thixotropic body from the starting values to steady state values. In the case of vesicular flow this corresponds to the deformation of bubbles from spherical to stretched shape. In a pure viscoelastic body, stresses increase from 0 to a finite value $\mu \cdot \dot{\gamma}$. The combined response may be with or without overshoot in shear stresses. If $Cd > 0$ the time scale of thixotropic relaxation becomes faster and the combined response curve has an overshoot. The return of deformed vesicles to a spherical shape depends on how long a lava flow was at rest or at a small strain-rate. Typically, this will take place when the topographic gradient decreases. Finally, the overall rheological behaviour of lavas may be described by a stress–strain-rate equation of a particular mechanical model (Maxwell or Jeffrey's body)

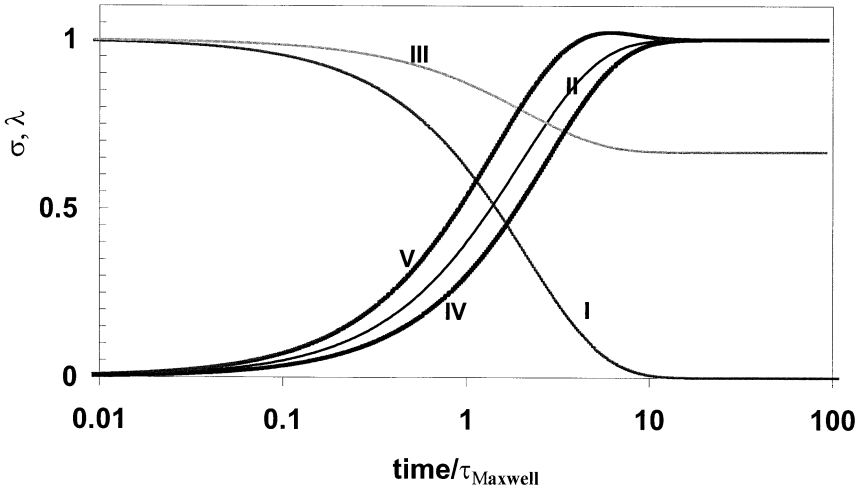

Fig. 10. Response of viscoelastic thixotropic material to an applied pulse of shear rate as a function of time in $\tau_{Maxwell}$ units, where $\tau_{Maxwell}$ is a viscoelastic relaxation time $\sim \mu/G$: (I) deformation parameter of vesicles in the melt, $Cd = 0$; (II) pure viscoelastic response; (III) pure thixotropic response; (IV) combined response; (V) combined response at $Cd = 1$. Stresses are scaled to the maximum stress. For details of calculation see text.

combined with a kinetic equation of a structural parameter λ. The overall response of lava flow to a change of slope is influenced by a combination of viscoelastic and thixotropic processes. The relative contribution of thixotropy to the shear stress relaxation depends on the volume fraction of vesicles. In a suspension $\phi \sim 10$ vol% the relative viscosity decreases by a factor of ~ 1.4, and when $\phi \sim 50$ vol% there is a 6-fold decrease in viscosity (Rust and Manga, 2002b). This effect is smaller in comparison with the effect of crystallinity. At $\phi \sim 10$ vol% crystals viscosity increase is 6 times, at 50 vol% the relative viscosity increase is 22 times (Pinkerton and Stevenson, 1992). In order to observe the combined effects arising from thixotropic and viscoelastic responses at the cessation of a strain-rate, the time scales of bubble shape relaxation (τ) and Maxwell time ($\tau_{Maxwell}$) must be of the same scale. Because of a very high unrelaxed shear modulus of silicate melts ~ 10 GPa, $\tau \gg \tau_{Maxwell}$. The exception may be suspensions with high volume fraction > 50 vol%. The rate of thixotropic relaxation after imposing a strain-rate or in accelerated flow depends on Ca and Cd. When these parameters are high, the rate of thixotropic relaxation may be comparable with a rate of viscoelastic relaxation. Thus, thixotropy remains a principle mechanism for transient lava flows on a variable topography.

(2) Most lavas are partially crystallised melts. The tendency of crystals to flocculate when magma is at a rest or subjected to a small strain-rate can induce a yield strength in the lava. This can subsequently be destroyed by shearing, for example when the slope increases. This is therefore another mechanism for inducing thixotropy in lavas. Numerical modelling reveals how a continuous crystal network in magmas may result in a finite yield strength when the crystal volume fraction becomes critical (Pinkerton and Stevenson, 1992). The critical volume fraction becomes smaller when the elongation shape factor of crystals is larger (Saar et al., 2001).

When lavas are subjected to small strain-rates (or small stresses) the overall rheology is determined by the deformation of gas bubbles and the rotation, interaction and displacement of crystals suspended in the viscous melt matrix. Internal stresses from friction and interaction between crystals are responsible for the formation of a yield strength. At higher strain-rates, e.g. when applied shear stresses are higher than the yield strength, apparent viscosities (defined here as $\sigma/\dot{\gamma}$) and effective viscosities (defined here as $\Delta\sigma/\Delta\dot{\gamma}$) are reduced. The observed effective viscosity at high strain-rates and stresses has a plastic character. In other words, yield strength lavas demonstrate a solid-like viscoelastic behaviour at low stresses and at low strain-rates and a plastic liquid-like behaviour at high stresses. The experiments with Gum rosin have revealed a low-frequency plateau for a shear modulus and may be correlated with a yield strength of this material. In lavas the yield strength can be explained by a building a network structure of touching crystals and vesicles. The effect of crystal anisotropy or aspect ratio of smallest and largest diameters has been considered by Saar et al. (2001). It was demonstrated that the yield strength of a suspension becomes appreciable after a critical concentration of particles in vol% ϕ_c. The threshold of particle concentration depends on the parameter λ as ϕ_c (see Saar et al., 2001, fig. 5). The yield strength σ_Y depends on particle concentration and a maximum packing of crystals ϕ_m as follows:

$$\sigma_Y = 5.3 \cdot \left(\frac{\frac{\phi}{\phi_c} - 1}{1 - \frac{\phi}{\phi_m}} \right) \tag{8}$$

(Hoover et al., 2001). Assuming the maximum packing parameter $\phi_m \sim 65$ vol% for a vesicular suspension, we get for $\phi \sim 50$ vol% a yield stress $\sigma_Y = (7.6 \cdot \lambda^{-0.52} = 4.3)$ in Pa. In a vesicular suspension the yield strength increases with time or deformation of vesicles ($\lambda \sim 0$) and after the cessation of a flow it relaxes to small values again. This effect is important when a vesicular flow decelerates or when a topographic slope becomes more shallow because σ_Y relaxes from high ($K \cdot Ca^m > 1$) to low value ($K \cdot Ca^m < 1$) due to thixotropic relaxation of λ. Thus, in high porosity lavas ($\phi > 30$ vol%) the yield strength is due to stretching of vesicles. Eq. 8 cannot be used to access quantitatively the yield strength of vesicular flow. In the model of Saar et al. (2001) ϕ_c as a function of λ

has been calculated assuming a random orientation of non-spherical inclusions. In the case of vesicles a shear flow imposes a steady state orientation of bubbles (Rust and Manga, 2002b). Realistic values $\phi_c(\lambda)$ for deformed vesicles must be larger than for solid particles. Lavas with high porosity have both a yield strength and viscoelasticity and are consequently highly non-Newtonian.

(3) From a series of experiments with a soap foam we demonstrated that an aqueous foam possesses both viscoelastic properties and a yield strength. Our step in shear experiments has shown that a mechanical model of the viscoelastic response of a foamed material with a yield strength can be constructed (Fig. 11A). The mechanical model describing viscoelastic response of foams and vesicle suspensions is more complicated than a Maxwell body model, for example, a 3-parameter body (Llewellin et al., 2002), or a 4-parameter body (Bagdassarov and Dingwell, 1993; Bekkur and Scrivener, 1998). The suggested mechanical model consists of elasto-plastic element and a viscous element. At small stresses the response is only elastic due to the elastic deformation of vesicles having an effective shear modulus $\sim 2\Gamma/a$. At stresses higher than the yield strength, the response is viscoelastic. The viscous and elastic elements are strain-rate dependent. The viscosity is shear thinning $\mu \propto (\dot{\gamma})^{-0.8}$ in the accessible span of shear rates, and the shear modulus depends on strain-rate as $G = G(\infty) \cdot ((\tau\dot{\gamma})^{1.6}/1 + (\tau\dot{\gamma})^{1.6})$. These results compare well with previous measurements on suspensions and foams (Prud'homme and Khan, 1996) where the power law dependence of oil–water suspension at ca. 90 vol% of vesicles was estimated ~ -0.8. The estimation of yield strength is 5 Pa assuming surface tension $\Gamma = 0.08$ N/m and $a = 10^{-3}$ m. (Prud'homme and Khan, 1996, eq. 15). The response of a foam is elastic at stresses less than the yield strength. When $\sigma > \sigma_y$, the shear stress relaxes due to stretching of bubbles. After removal of external applied stress, the elastic stress does not decrease to zero. In this model the foam possesses a shear modulus comparable with the yield strength.

At high concentrations of vesicles in a fluid the rheological behaviour of different suspensions is very similar (for example, compare Prud'homme and Khan (1996) and this study). This may suggest that the mechanical model shown in Fig. 11A is also true for magmatic foams. Consequently, transient thixotropic flow, shear thinning and

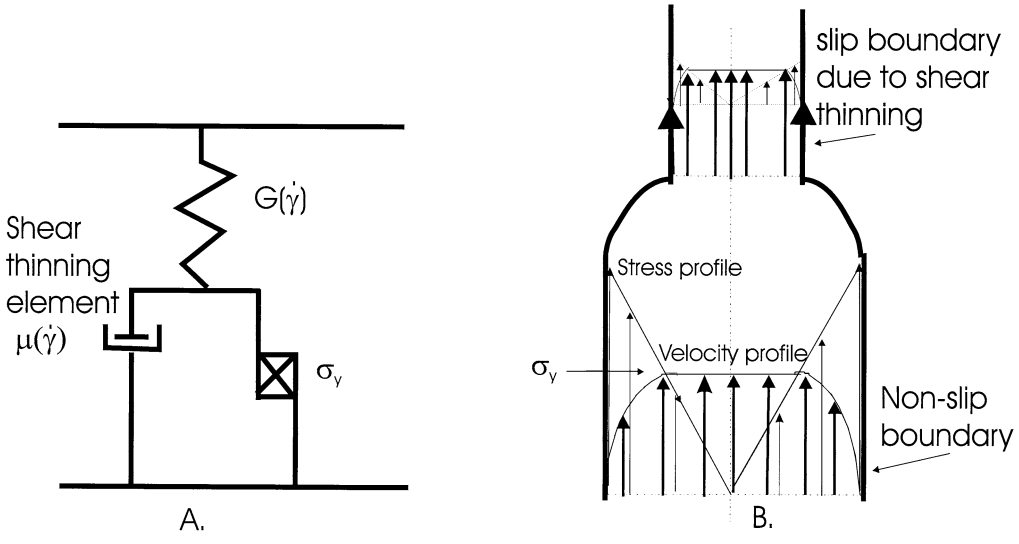

Fig. 11. The sketch of a viscoelastic model for magma-foam (A) and the profile of a shear stress and velocity distribution (B) near an abrupt orifice in a magma conduit.

the existence of a yield strength may play significant roles in the detachment of magma in conduits (Fig. 11B). In a relatively large magma conduit there is a non-slip boundary condition for magma velocity on the wall of the channel. When this flow meets a narrowing region in the channel, then, as a consequence of the shear-thinning rheology of the magma, high shear stresses cannot build up near the wall because the product of *strain-rate x viscosity* is practically constant for a foam. At the same time the core of the flow cannot accelerate because of the yield strength which is important in a central core region where shear stresses are small (Fig. 11B). In order to provide the same volumetric rate of flow in a wide region and in narrow region of the conduit, there should be transition from non-slip to slip boundary conditions on the wall. A continuous flow of magma has to transform at this point into a pulsating flow, which has been observed in shock tube experiments on Gum rosin-acetone foams (Phillips et al., 1995). Natural magma and channels have rough and irregular geometries. Assuming a certain wavelength of channel wall roughness, this transient flow may result in an emission of acoustic waves.

Fig. 12 illustrates the effect of the yield strength and shear thinning on a flow of fluid at the entrance of a narrow orifice. The transition of the flow from the regime of slip (b) to non-slip boundary conditions (c) occurs when a dimensionless parameter ($D\sigma_Y/\bar{v}\mu \sim 2.5$–$2.7$, where D is the diameter of the large tube, $\bar{v}$ is a mean flow velocity, and σ_Y is yield strength (Barnes, 1999). Field measurements on Etnean lavas at 1095°C yield a plastic viscosity of 1260 Pa s and a yield strength of 370 Pa (Pinkerton and Norton, 1995). At a mean velocity of 0.5 m/s the non-slip to slip boundary transition may occur in a conduit 4.5 m in diameter. Deformation of a yield strength lava is mostly restricted to a near-wall region, but at the entrance of any narrow orifice all the material has to flow in order to enter the channel. Therefore, the non-slip boundary condition must be violated and a portion of fluid has to be detached from a conduit wall. We propose that this process can account for the periodic detachment of foam in the decompression experiments with foamed

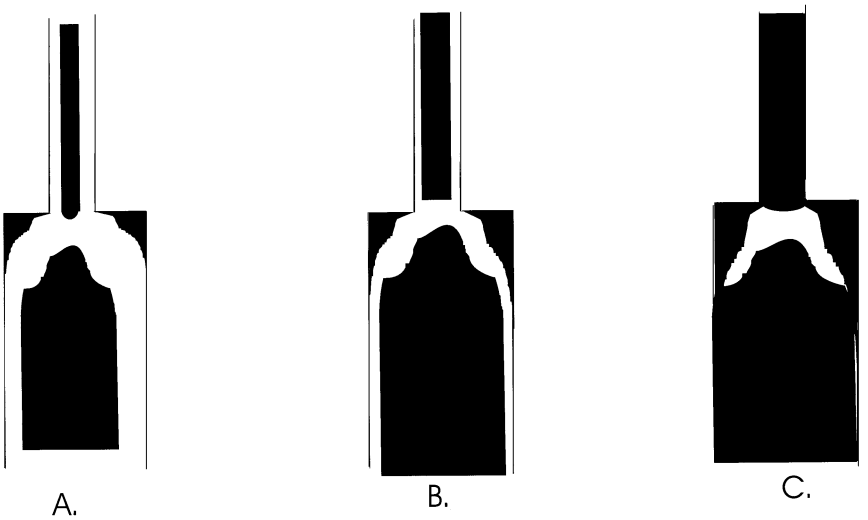

Fig. 12. Sketch of pulsating magma flow of fluid through an abrupt orifice (ratio of diameters 1:4) for differing values of yield strength (redrawn from Barnes, 1999). From (A) to (C) the yield strength increases. Black indicates the region where the stress is below the yield strength. White is where stresses exceed the yield strength. Viscous flow of magma is only possible in this region. After closing the conduit (C), the build-up in stress caused by expanding foam will return the system to the initial situation (A). The overall regime of flow through a narrowing orifice has a pulsating character with transition from slip-free and slip boundary conditions on the conduit wall.

Gum rosin (Phillips et al., 1995). Similar effects may be expected for a flow of a decompressed magma in a volcanic conduit assuming that walls of a channel have a roughness of a certain wavelength.

Acknowledgements

The authors thank G. Ryan for undertaking the gum rosin torsion experiments and S. Lane for the discussion of the shock tube decompression experiments. Comments of C. Kilburn and an anonymous reviewer helped to improve the manuscript. The authors are grateful to DAAD for the travel grants of exchange programme between Lancaster University and the University of Frankfurt.

Appendix

The semi-empirical model adequately describing the rheology of bubbly suspension has been proposed by Llewellin et al. (2002) on the basis of the linear Jeffrey's model parameterised to empirically determined constants on the gas volume fraction ϕ:

$$\sigma + \frac{6\tau}{5}\sigma = \mu(1+9\phi)\dot{\gamma} + \mu\frac{6\tau}{5}\left(1-\frac{5}{3}\phi\right)\ddot{\gamma}, \qquad \text{(A1)}$$

where τ is a bubble shape relaxation time $\tau \sim (a \cdot \mu / \Gamma)$, μ is a shear viscosity of the liquid phase, Γ is surface tension and R is the vesicle radius. The data have been obtained at $Ca \ll 1$. The Jeffrey's model represents a viscous dash-pot connected in parallel with a Maxwell element or a dash pot in series with a Kelvin element. The theory of the viscoelastic response of Jeffrey' body is described elsewhere (e.g. Cheng, 1982). This body may express a normal thixotropy, if the slope of viscosity of the equilibrium flow curve is less than that of the constant structure flow curve (see Fig. 2). The response of a Jeffrey' body to a step function of a strain-rate has an overshoot on the shear stress–time curves. The overshoot is due to an overlapping of viscoelastic retarded growth of stress of a slower dash-pot with a thixotropic breakdown of a structure (faster dash-pot of Kelvin element). This may occur when a shear modulus of a bulk melt is about the same as $\Gamma/2R$. This type of response has been observed experimentally in a vesicular rhyolite by Bagdassarov and Dingwell (1993), and they also suggested a four-parameter body model for a stress relaxation in vesicular rhyolite melt. They considered two different stress relaxation time scales associated with μ/G and $\mu \cdot a/G$ where G is an unrelaxed shear modulus of melt.

According to Eq. A1, the non-spherical stretched bubbles will reduce viscosity when the dynamic Capillary number $Cd = \tau(\ddot{\gamma}/\dot{\gamma})$ is significantly larger than 1 (Llewellin et al., 2002). If Cd is high (as in the case of an accelerated lava flow), the second term in Eq. A1 dominates in the overall stress evolution and the effective viscosity of a flow decreases with the increase of bubble content. For a lava flow on the slope of a volcano, the reason for the flow acceleration or sudden increase of Cd can be an abrupt change of a topography, i.e. a change of the slope along the lava flow length. At onset of flow acceleration, stretching may additionally increase the effective velocity of the flow making a lava material on a steep topography catastrophically fluid. According to the standard solution of a viscous flow on a inclined plane accounting a variable thickness h along the slope length L (Landau and Lifshitz, 1987; Miyamoto and Sasaki, 1998), the expressions for the strain-rate ($\dot{\gamma}$) and the strain-rate acceleration ($\ddot{\gamma}$) can be written as follows:

$$\dot{\gamma} = \frac{\rho g\left\{\sin\alpha - \frac{dh}{dL}\cdot\cos\alpha\right\}}{\mu}(h-z), \qquad \text{(A2)}$$

and:

$$\ddot{\gamma} = \frac{v(z)\rho g}{\mu}\left[\left(\frac{d\,\sin\alpha}{dL} - \frac{dh}{dL}\left(\frac{dh}{dL}\cdot\cos\alpha\right)\right)\right.$$

$$\left.(h-z) + \left(\sin\alpha - \frac{dh}{dL}\cdot\cos\alpha\right)\cdot\left(\frac{d(h-z)}{dL}\right)\right], \qquad \text{(A3)}$$

where $v(z)$ is a flow velocity profile, L is a length coordinate of a flow, h is a thickness of a flow. The dynamic Capillary number which will characterise the importance of the bubble stretching

process on a flow rheology may be expressed as follows:

$$Cd = \frac{a}{2\cdot\Gamma}\cdot\rho g\cdot z(2h-z)\cdot \left[\left(\frac{dA}{dL}\right) + \frac{A}{(h-z)}\cdot\left(\frac{d(h-z)}{dL}\right)\right], \quad \text{(A4)}$$

where:

$$A = \sin\alpha - \frac{dh}{dL}\cdot\cos\alpha. \quad \text{(A5)}$$

The dynamic Capillary number consists of the variation of a topographic angle along a lava flow distance (the first term in brackets of r.h.s. of Eq. A4) and of the variation of the thickness of a flow (the second term in brackets). The latter term may be neglected in comparison with the first one as a small logarithmic derivative. Eq. A4 shows that the main effect on the bubbly flow rheology comes from large bubbles stretched in the upper part of a flow. The useful approximation of the dynamic Capillary number for lava flows with nearly constant thickness h is:

$$Cd = \frac{a\cdot\rho\cdot g\cdot h^2}{2\cdot\Gamma}\cdot\frac{d\sin\alpha}{dL}. \quad \text{(A6)}$$

Assuming $h\sim 5$ m, $a\sim 2\cdot 10^{-2}$ m, $\Gamma\sim 0.3$ N/m (Bagdassarov et al., 2000), $\rho\sim 2.5\cdot 10^3$ kg/m^3, only a variation of the slope angle greater than 10^{-2} rad/m results in $Cd\sim 10$. This may already cause a transition to a stretching process of vesicles in lava flow and in a decrease of the plastic flow viscosity.

References

Avramis, K.S., Turian, R.M., 1991. Yield stress of laterite suspensions. J. Coll. Interface Sci. 143, 54–68.

Bagdassarov, N., 2000. Anelasticity and viscoelasticity of partially molten rocks and lavas. In: Bagdassarov, N.S., Laporte, D., Thompson, A. (Eds.), Physics and Chemistry of Partially Molten Rocks. Kluwer Academic Press, Dordrecht, 272 pp.

Bagdassarov, N.S., Dingwell, D.B., 1993. Deformation of foamed rhyolites under internal and external stresses: Experimental investigation. Bull. Volcanol. 55, 147–154.

Bagdassarov, N.S., Dorfman, A.M., Dingwell, D.B., 2000. Effect of alkalis, phosphorus, and water on the surface tension of haplogranite melt. Am. Mineral. 85, 33–40.

Barnes, H.A., 1997. Thixotropy – a review. J. Non-Newtonian Fluid Mech. 70, 1–33.

Barnes, H.A., 1999. The yield strength – a review or 'παντα ρει' – everything flows? J. Non-Newtonian Fluid Mech. 81, 133–178.

Bautista, F., de Santos, J.M., Puig, J.E., Manero, O., 1999. Understanding thixotropic and antithixotropic behaviour of viscoelastic micellar solutions and liquid crystalline dispersions, I. The model. J. Non-Newtonian Fluid Mech. 80, 93–113.

Bekkur, K., Scrivener, O., 1998. Time-dependent and flow properties of foams. Mech. Time-Depend. Mater. 2, 171–193.

Cheng, D.C.H., 1974. On the behaviour of thixotropic fluids with a distribution of structure. J. Phys. D 7, L155–L157.

Cheng, D.C.-H., 1982. Rotational Viscometers and Thixotropic Measurement. Warren Spring Laboratory, Report 62, Stevenage, 81 pp.

Cheng, D.C.H., 1986. Yield strength: A time-dependent property and how to measure it. Rheologica Acta 25, 542–554.

Cheng, D.C.H., Evans, F., 1965. Phenomenological characterisation of the rheological behaviour of inelastic reversible thixotropic and antithixotropic fluids. Br. J. Appl. Phys. 16, 1599–1617.

Dragoni, M., 1993. Modelling the rheology and cooling of lava flows. In: Kilburn, C.R.J., Luongo, G. (Eds.), Active Lavas. UCL Press, London, pp. 235–262.

Dragoni, M., Tallarico, A., 1996. A model for the opening of ephemeral vents in a stationary lava flow. J. Volcanol. Geotherm. Res. 74, 39–47.

Hoover, S.R., Cashman, K.V., Manga, M., 2001. The yield strength of subliquidus basalts – experimental results. J. Volcanol. Geotherm. Res. 107, 1–18.

James, M., Bagdassarov, N., Müller, K., Pinkerton, H., 2004. Viscoelastic behaviour of basaltic lavas. J. Volcanol. Geotherm. Res. doi: 10.1016/S0377-0273/03)00340-8.

Keszthelyi, L., Self, S., 1998. Some physical requirements for the emplacement of long basaltic lava flows. J. Geophys. Res. 103, 27447–27464.

Kouchi, A., Tsuchiyama, A., Sunagawa, I., 1986. Effect of stirring on crystallisation kinetics of basalt: Texture and element partitioning. Contrib. Mineral. Petrol. 93, 429–438.

Landau, L.D., Lifshitz, E.M., 1987. Theoretical Physics: Hydrodynamics, 2nd ed. Pergamon Press, New York, 730 pp.

Liddell, P.V., Boger, D.V., 1996. Yield strength measurements with the vane. J. Non-Newtonian Fluid Mech. 63, 235–261.

Lipman, P.W., Banks, N.G., Rhodes, J.M., 1985. Gas-release induced crystallization of 1984 Mauna Loa magma, Hawaii, and effect on lava rheology. Nature 317, 604–607.

Llewellin, E.W., Mader, H.M., Wilson, S.D.R., 2002. The rheology of bubbly liquid. Proc. R. Soc. Lond. A 458, 987–1016.

Manga, M., Loewenberg, M., 2001. Viscosity of magmas containing highly deformable bubbles. J. Volcanol. Geotherm. Res. 105, 19–24.

Manga, M., Castro, J., Cashman, K.V., Loewenberg, M., 1998. Rheology of bubble-bearing magmas. J. Volcanol. Geotherm. Res. 87, 15–28.

Marsh, B.D., 1981. On the crystallinity, probability of occurrence, and rheology of lava and magma. Contrib. Mineral Petrol. 78, 85–98.

Marsh, B.D., 1987. Magmatic Processes. Rev. Geophys. 25, 1043–1053.

Miyamoto, H., Sasaki, S., 1998. Numerical modelling simulations of flood basalt lava flows: Roles of parameters on lava flow morphologies. J. Geophys. Res. 103, 27489–27502.

Mourtada-Bonnefoi, C.C., Mader, H.M., 2001. On the development of highly-viscous skins of liquid around bubbles during magmatic degassing. Geophys. Res. Lett. 28, 1647–1650.

Mujumdar, A., Neris, A.N., Metzner, A.B., 2002. Transient phenomena in thixotropic systems. J. Non-Newton. Fluid Mech. 102, 157–178.

Nguyen, Q.D., Boger, D.V., 1992. Measuring the flow properties of yield strength fluids. Ann. Rev. Fluid Mech. 24, 47–88.

Norton, G., Pinkerton, H., 1997. Rheological properties of natrocarbonatite lavas from Oldoinyo Lengai, Tanzania. Eur. J. Mineral. 9, 351–364.

Pernell, C.W., Foegeding, E.A., Daubert, C.R., 2000. Measurements of the yield strength of protein foams by vane rheometry. J. Food Sci. 65, 110–114.

Phillips, J.C., Lane, S.L., Lejeune, A.-M., Hilton, M., 1995. Gum rosin acetone system as an analogue to the degassing behaviour of hydrated magmas. Bull. Volcanol. 57, 263–268.

Pinkerton, H., Norton, G., 1995. Rheological properties of basaltic lavas at sub-liquidus temperatures: Laboratory and field measurements on lavas from Mount Etna. J. Volcanol. Geotherm. Res. 68, 307–323.

Pinkerton, H., Sparks, R.S.J., 1978. Field measurements of the rheology of lava. Nature 276, 383–384.

Pinkerton, H., Stevenson, R., 1992. Methods of determining the rheological properties of magmas at sub-solidus temperatures. J. Volcanol. Geotherm. Res. 53, 47–66.

Pinkerton, H., Wilson, L., 1994. Factors controlling the lengths of channel-fed lava flows. Bull. Volcanol. 56, 108–120.

Princen, H.M., Kiss, A.D., 1986. Rheology of foams and highly concentrated emulsions, III. Static shear modulus. J. Coll. Interface Sci. 112, 427–437.

Prud'homme, R.K., Khan, S.A., 1996. Experimental results on foam rheology. In: Prud'homme, R.K., Khan, S.A. (Eds.), Foams: Theory, Measurements, and Applications. Dekker, New York, pp. 217–241.

Rust, A.C., Manga, M., 2002a. Effects of bubble concentration on the viscosity of dilute suspension. J. Non-Newtonian Fluid Mech. 104, 53–63.

Rust, A.C., Manga, M., 2002b. Bubble shapes and orientations on low Re simple shear flow. J. Colloid. Interface Sci. 249, 476–480.

Saar, M.O., Manga, M., Cashman, K.V., Fremouw, S., 2001. Numerical models of the onset of yield strength in crystal-melt suspensions. Earth Planet. Sci. Lett. 187, 367–379.

Shaw, H.R., 1969. Rheology of basalt in the melting range. J. Petrol. 10, 510–535.

Shaw, H.R., Wright, T.L., Peck, D.L., Okamura, R., 1968. The viscosity of basaltic magma: An analysis of field measurements in Makaopuhi lava lake, Hawaii. Am. J. Sci. 266, 255–264.

Shaw, H.R., 1972. Viscosities of magmatic silicate liquids: an empirical method of prediction. Am. J. Sci. 272, 870–893.

Smith, J.V., 1997. Shear thickening dilatancy in crystal-rich flows. J. Volcanol. Geotherm. Res. 79, 1–8.

Sparks, R.S.J., Pinkerton, H., 1978. Effect of degassing or rheology of basaltic lavas. Nature 276, 385–386.

Spera, F.J., Borgia, A., Strimple, J., 1988. Rheology of melts and magmatic suspensions, 1. Design and calibration of concentric cylinder viscometer with application to rhyolitic magma. J. Geophys. Res. 93, 10273–10294.

Stein, D.J., Spera, F.J., 1992. Rheology and microstructure of magmatic emulsions: Theory and experiments. J. Volcanol. Geotherm. Res. 49, 157–174.

Stein, D.J., Spera, F.J., 2002. Shear viscosity of rhyolite-vapor emulsions at magmatic temperatures by concentric cylinder rheometry. J. Volcanol. Geotherm. Res. 113, 243–258.

Stevenson, R.J., Bagdassarov, N.S., Romano, C., 1997. Vesiculation in a water-rich calc-alkaline obsidian. Earth Planet. Sci. Lett. 146, 555–571.

Stevenson, R.J., Dingwell, D.B., Bagdassarov, N.S., Manley, C.R., 2001. Measurement and implication of 'effective' viscosity for rhyolite flow emplacement. Bull. Volcanol. 63, 227–237.

Turian, R.M., Ma, T.W., Hsu, F.L.G., Sung, D.J., 1997. Characterisation, settling, and rheology of concentrated fine particulate mineral slurries. Powder Technol. 93, 219–233.